

An Iterative Machine-Learning Framework for Turbulence Modeling in RANS

Weishuo Liu^a, Jian Fang^{b,*}, Stefano Rolfo^b, Charles Moulinec^b, David R Emerson^b

^a*School of Energy and Power Engineering, Beihang University, 37 Xueyuan Road, Haidian District, Beijing, 100191, China*

^b*Scientific Computing Department, Science and Technology Facilities Council Daresbury Laboratory, Keckwick Lane, Daresbury, Warrington, WA4 4AD, UK*

Abstract

Machine-learning (ML) techniques provide a new perspective for constructing turbulence models for Reynolds-averaged Navier–Stokes (RANS) simulations. Designed with advanced fitting ability, they can increase the accuracy of the turbulence models given enough information from high-fidelity datasets is provided. In this study, an iterative ML-RANS computational framework is proposed, that combines the ML algorithm and transport equations of a conventional turbulence model built on empirical knowledge. This framework could maintain a consistent procedure to obtain the input features for ML models in both the training and predicting stages. The effective form of the closure term is discussed to explain how to determine the target variables for the ML algorithm, which ensures a mean flow solution of RANS equations free of amplified error. The inherent multi-valued problem of the existing constitutive theory is studied to establish a proper regression system for ML algorithms. From the same input features, an accurate closure can be obtained through ML model, and a flow field similar to the high-fidelity datasets can be obtained based on such closure, so that a built-in reproducibility for the training cases can be achieved. It is demonstrated that the framework can deal with a cross-case training strategy with data from turbulent channel flows at different Reynolds numbers. *A posteriori* simulations of channel flows show that the framework is able to predict both the mean flow field and turbulent variables accurately. Applied to the flow over periodic hills a better result than for a conventional first order turbulence model is obtained, indicating a promising prediction capability of the developed ML-RANS model for a recirculating flow even though the model is trained with planar channel flow data.

Keywords: RANS, Machine Learning, Turbulence Modeling

*Corresponding author.

Email addresses: liuweishuo@buaa.edu.cn (Weishuo Liu), jian.fang@stfc.ac.uk (Jian Fang), stefano.rolfo@stfc.ac.uk (Stefano Rolfo), charles.moulinec@stfc.ac.uk (Charles Moulinec), david.emerson@stfc.ac.uk (David R Emerson)

1. Introduction

The Reynolds-averaged Navier–Stokes (RANS) equations have been widely used for decades in fluid engineering and will continue to play an essential role because of their reduced computational cost [1, 2]. However, averaging the Navier–Stokes equations creates new Reynolds stress terms implying a closure problem. Over a hundred years, a large number of turbulence models have been developed [3, 4, 5, 6, 7, 8, 9, 10] with a physics-driven modeling process, relying on hypothesis based on physical intuition, constructing transport equations, parameterizing the models and calibrating the coefficients. The advantage of these physics-driven models is that they can grasp the major turbulence transport characteristics, and can be successfully applied to a broad range of engineering scenarios. But still, the turbulence model is yet the primary source of the uncertainty in RANS simulations [11, 12, 13, 14], because of the limitation of traditional modeling techniques and the deviation from the preset ideal conditions in real engineering scenarios.

Recently, the machine learning (ML) technique, as an efficient tool to deal with complex regression systems [15], sheds light on the RANS closure problem by providing an alternative data-driven method to establish the mapping relation between the closure term and mean flow field. Therefore, the closure problem can be solved using a data-driven methodology. Some latest studies have proven the feasibility of the application of ML algorithms in turbulence modeling [16, 17] utilizing data from high-fidelity simulations.

Generally speaking, a turbulence model is constructed with a combination of transport equations and an algebraic constitutive law to calculate the Reynolds stress tensor [18, 8], such as the first order ones using two-equation models [9, 10, 4, 5, 6].

In terms of transport equations, Parish & Duraisamy [19] and Holland *et al.* [20] developed a field inversion technique to find the spatial distribution of the ML target variables. This strategy, combined with an ML technique such as the artificial neural network (ANN), was used to construct a functional form of correction coefficients in the turbulence transport equations. The methodology was applied and tested for the S – A model [21, 22, 23] and the transitional k – ω model [24, 22]. Successful reproductions of the training cases were achieved even if how they trained their data from experimental data. Besides, Zhu *et al.* [25] explored the possibility to substitute the partial differential equation (PDE) in the S – A model with an algebraic mapping in ANN, demonstrating a promising fitting ability of the ML model.

As for the constitutive law, existing studies mainly followed the general effective-viscosity hypothesis and the mathematical form originally proposed by Pope [26]. Under this form, the dimensionless deviatoric Reynolds stress tensor is expressed as a function of dimensionless mean strain tensor and rotation tensor, which leads to a linear combination of a series of integrity tensor basis under the theory of tensor analysis [27] and matrix polynomials [28, 29]. Each combination coefficient can be expressed as a function of the invariance of the series of integrity tensor basis. However, the calibration of the coefficients of the functional remains the major problem of this. Weatheritt & Sandberg [30, 31] worked on a novel parametric modeling approach. They utilized a gene expression program to search for an optimal analytical formula for coefficients of the tensorial combination. Favorable algebraic expressions were respectively found for separated flows [30] and duct flows [31], and the

application of their model trained with data from low-pressure turbine wake flow showed an improvement against isotropic models [32].

Besides, the functional mapping of the coefficients could also be estimated by a non-parametric ML model. Ling *et al.* [33] firstly introduced a neural network with a specified structure, embedded tensorial invariance in the structure of the ML model [34]. Wang *et al.* [35] and Wu *et al.* [36] extended the constitutive expression with two more tensors and used the random forest algorithm to select the most relevant features. Both studies provided valuable modeling methodologies and showed improved predictions of anisotropic flows against linear constitutive models. However, the prediction yielded a one-step augmentation instead of an iteratively converged simulation. The closure term was predicted based on the mean flow field of a RANS simulation, and was frozen after the prediction. The final result was obtained by further running the RANS equations with the frozen closure term. This means that the results of their studies still could be seen as intermediate flow fields instead of the dynamical fixed point of the ML-integrated PDE system. As the closure term was not frozen but dynamically updated with the simulation, the simulation could deviate from the result presented in their studies. Therefore, the design of the computational process and internal technical details need to be further investigated and developed.

In Ling’s framework [33, 34], there existed an inconsistency between the turbulence quantities (e.g., k and ϵ) used in the training and predicting stages. In the training process, statistically averaged turbulence quantities (e.g., k , ϵ) from the high-fidelity database were directly used to obtain the training data. Whereas in the prediction process, the ML model was actually giving predictions based on turbulence quantities estimated by traditional turbulence models. As a consequence, structural uncertainties were introduced into the framework by the different procedures to obtain turbulence quantities between training and predicting stages. Apart from this, the primary hypothesis of the general effective-viscosity theory of Pope [26] used by Ling *et al.* [33, 34] appeared to be a multi-valued function (see Sec. 2.3). This multi-valued problem could lead to great difficulty for the ML regression models deterministic relationship, and could potentially destroy the continuity of the machine-learned functional mapping, which is essential in a PDE system.

In contrast, the physics-informed ML framework of Wang *et al.* [35] and Wu *et al.* [36] introduced more independent tensors into the constitutive relations, as they derived an eddy-viscosity-based decomposition form of the closure term to ensure the consistency between a model’s *a priori* and *a posteriori* performances [37]. However, the computational architecture was compromised into an open-loop process. During the training process of the ML model, conventional RANS mean flow features were used as input, and closure terms from high-fidelity simulations were used as a training target. Therefore, the mapping relation was actually constructed between an inaccurate mean flow and an accurate closure term, which brought difficulties in predicting global flow phenomena such as the area of a separation region. The possible reason for the loss of the convergence could have been the choice of the random forest algorithm, which is actually a sum of simple step functions with an intrinsic absence of continuity and differentiability, when applied to a PDE system.

In the presented research, we aim at constructing a computational framework iterating between the ML model and the RANS solver. The major challenge is to ensure that the

same solution as the high-fidelity mean flow field can be obtained within the design of the computational framework. Firstly, the input features in the training and predicting stages should be obtained with the same procedure. To achieve this objective, transport equations from a traditional turbulent model are used to process on the high-fidelity mean flow field to obtain an empirical estimation of turbulence quantities, because the turbulence quantities defined by the ensemble averaged fluctuation fields are not computationally reachable by the resolution of RANS simulation. Then the estimated turbulence quantities are combined with the high-fidelity mean flow to form the input features, so that the constituent parts of inputs are all computed by the RANS simulation. Secondly, the deterministic ML algorithms (e.g., the ANN, random forest, etc.) are essentially algebraic functions, which can only embed functional mappings with uniquely determined function values. Therefore, the multi-valued problem in the previous constitutive relations needs to be fixed with the extended set of independent variables. This is required to get a proper regression system and for the ML model to be trained successfully. A functional mapping between the correct mean flow and the closure term can thus be constructed. Finally, the form of the closure term and the way how it is integrated into the RANS equations also has an impact on the robustness of the PDE system regarding the statistical errors. Here the eddy-viscosity-based decomposition of the closure term [37] is used in this study to improve the conditioning of the RANS equations, because they can suffer from an ill-conditioning problem if the Reynolds stress tensor is directly introduced as a source term. The eddy-viscosity-based closure ensures that statistical errors in closure terms would not be propagated into the solution, and that could finally lead to a solution in good agreement with the high-fidelity mean flow field. A built-in reproducibility of the training cases can thus be achieved through the above design of the ML-RANS framework.

In this study, Direct Numerical Simulation (DNS) data of turbulent channel flows are used to demonstrate the multi-valued problem under the simplest form of the general constitutive relation. Such a database is used to train the ML models following a cross-case strategy, where data at different Reynolds numbers are merged together and fed to the ML model at the same time. The model trained for the channel flow is not only able to give accurate results for channel flows at Reynolds numbers within the training range, but also can better predict a separated flow than a well-established RANS model, illustrating a promising prospect of the developed framework.

The paper is organized as follows. The methodology is introduced in Sec. 2, with the structure of the developed ML-RANS framework and a brief discussion on the necessary measurements to take for a reproducibility of the training cases (Sec. 2.1). Then the two major challenges, the effective form of the closure term and the multi-valued problem of the general constitutive hypothesis, are discussed in Sec. 2.2 and Sec. 2.3 respectively. The training results and the *a posteriori* tests of the developed ML model are shown in Sec. 3, and conclusions are drawn in Sec. 4.

2. Methodology

An iterative ML-RANS framework is proposed to derive a consistent procedure to obtain the turbulence quantities used in the training and prediction stages. Within the framework, two significant topics in ML-based turbulence modeling, including the effective form of the closure term and the multi-value problem in existing constitutive relations, are discussed based on previous research and data analysis in a turbulent channel flow.

2.1. Iterative ML-RANS Framework

The Reynolds averaged Navier-Stokes equations for incompressible flow of non-Newtonian fluid written for steady state read

$$\begin{aligned}\nabla \cdot \mathbf{u} &= 0 \\ \mathbf{u} \cdot \nabla \mathbf{u} - \nu \nabla^2 \mathbf{u} + \nabla p - \nabla \cdot \boldsymbol{\tau} - \mathbf{f} &= 0\end{aligned}\tag{1}$$

where \mathbf{u} is the mean velocity vector, ν is the molecular viscosity, p is the mean pressure, the term $\boldsymbol{\tau}$ is the unclosed Reynolds stress tensor and \mathbf{f} is the body force acting on the continuum.

When the steady state RANS equations are solved in an iterative manner [38, 39], the procedure refers to solving the turbulence transport equations and applying a constitutive relation (except for Reynolds Stress Models, which adopt a tensorial transport equations for each component of the Reynolds stresses so that the constitutive law is no longer needed). The procedure is shown as follows, in which the subscript n represents the solution for current the iteration and $n - 1$ for the previous iteration.

1. The initial mean velocity and pressure fields, namely \mathbf{u}^0 and p^0 , respectively are given, as well as the initial turbulence quantities.
2. The coefficients in the constitutive relation (e.g., the eddy-viscosity ν_t) are calculated based on the turbulence quantities at the previous iteration.
3. The momentum equations with continuity correction including a pressure Poisson's equation for the pressure are solved using closure term and mean field (\mathbf{u}^{n-1} , p^{n-1}) from the previous iteration. The mean flow field is then updated to (\mathbf{u}^n , p^n).
4. The turbulence transport equations are solved based on the mean field (\mathbf{u}^n , p^n).
5. If the simulation has not converged, go back to Step 2.

The ML regression technique can be integrated into this computational process at either Step 2 or Step 4 for the calculation of an effective closure term. In this study, we implement the ML model at Step 4 to assist the calculation of the closure term. Dimensionless functional mapping is embedded into the ML model, where the input features consist of the mean flow field and transport-equation-estimated turbulence quantities. The overall process including training and predicting stage is shown in Fig. 1.

In the training stage, the input feature and target variables for the ML model are obtained from the training data, which are usually high-fidelity DNS data. The local turbulence quantities, such as the kinetic energy and dissipation rate used in the presented framework,

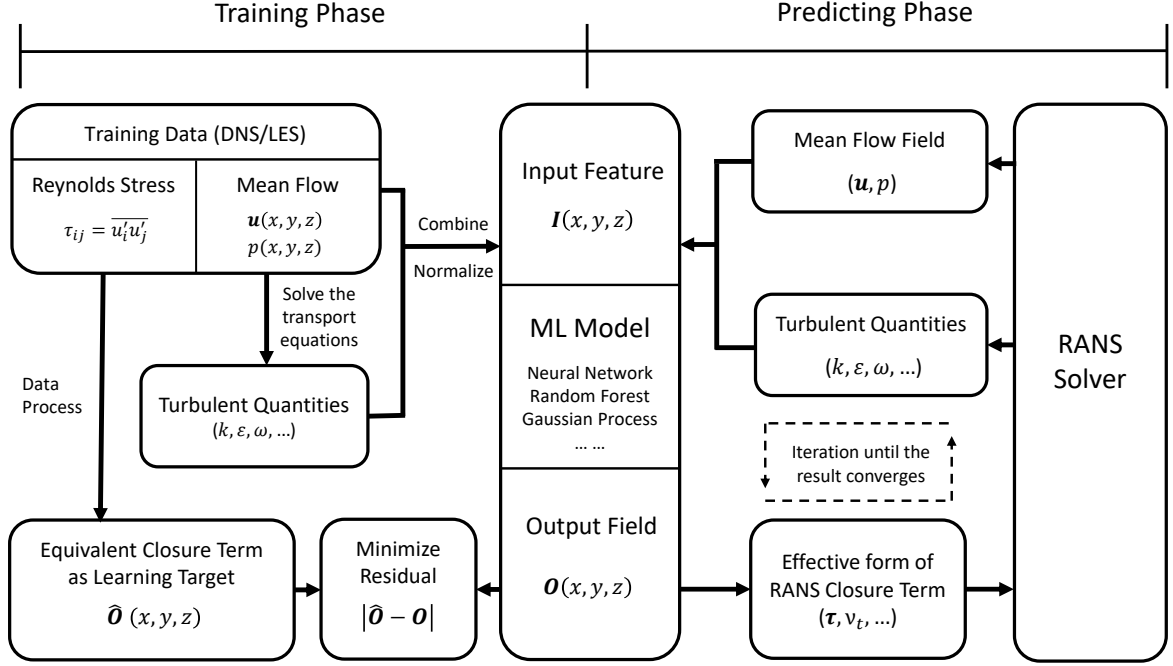


Figure 1: A comprehensive sketch for the iterative ML-RANS framework

are not calculated directly from the DNS data according to their physical definition, which is different from previous ML-RANS framework [33, 36, 35]. Instead, they are obtained by solving the transport equations of a traditional turbulence model based on the high-fidelity mean flow field.

Then the input features of the ML model, $\mathbf{I}(x, y, z)$, are calculated and normalized by combining the mean flow field and estimated turbulence quantities. This procedure ensures the consistency of the input features in training and predicting the various processes. The target variables of the output data for the ML model are processed from the statistically averaged Reynolds stresses of high-fidelity DNS data, and a non-dimensional equivalent form of the closure term is then calculated as $\hat{\mathbf{O}}(x, y, z)$. The data pairs $\{\mathbf{I}, \hat{\mathbf{O}}\}$ are fed into the ML model at the training stage. And the training process is finished when the error between the ML model's outputted $\mathbf{O}(x, y, z)$ from the ML model and the target $\hat{\mathbf{O}}(x, y, z)$ achieves the given tolerance. By the end of the training stage, an accurate mapping $\mathbf{O} = f(\mathbf{I})$ is established to support the calculation of the closure term.

In the prediction stage, the ML model obtained from the above training stage is loaded to a CFD solver. At each iteration step, the ML model receives the input field $\mathbf{I}(x, y, z)$ calculated by the CFD solver and returns the output field $\mathbf{O}(x, y, z)$ for the calculation of the closure term. The CFD solver then receives the output from the ML model, updates the closure term, and solves the RANS equations to get the mean flow field and turbulent

quantities used for the next step. The iterative loop keeps going until the residuals converge to the given tolerance.

Moreover, with the high-fidelity mean flow field mapped as the initial field, the solution of the ML-integrated RANS solver should be the same as the high-fidelity results, so that a built-in reproducibility of the training cases can be achieved. By analyzing the prediction phase of this computational framework shown in Fig. 2, if the mean flow field from high-fidelity simulations is mapped as the initial field, the structural design could ensure the same input vectors \mathbf{I} for the ML model (steps in Circle 1), since the input vector \mathbf{I} for training data is obtained in the same procedure. And to further obtain the same flow field as the high-fidelity simulations, two significant challenges also need to be discussed and ensured

- What equivalent form of closure term (as the learning target for ML models) is able to lead the RANS solver to converge to the mean flow field of the high-fidelity simulations (Circled 3 in Fig. 2)?
- Can a successful functional mapping $\mathbf{O} = f(\mathbf{I})$ be established throughout ML algorithms (Circled 2 in Fig. 2)?

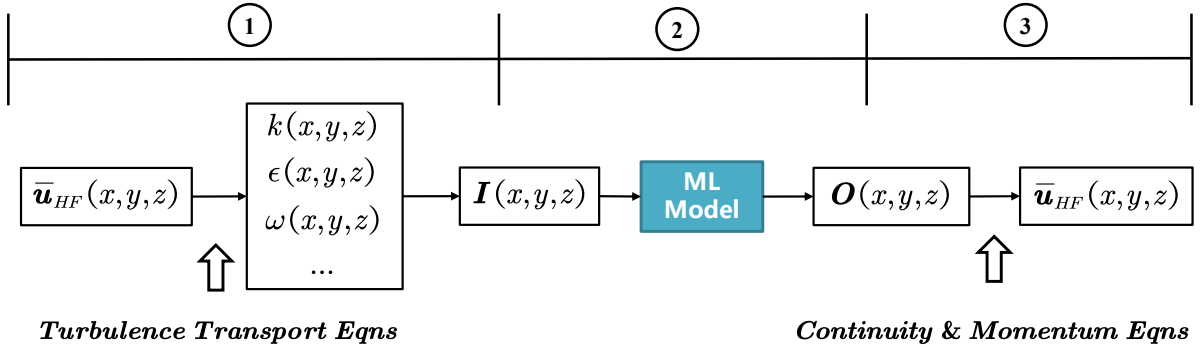


Figure 2: Prediction phase in iterative ML-RANS framework given HF mean flow as initial field. The design of the framework should satisfy the following requirements (1) the procedure’s consistency of obtaining the input vector \mathbf{I} . (2) the functional mapping relation $\mathbf{O} = f(\mathbf{I})$ can be established successfully. (3) the effective equivalent form of closure term mapped into the flow domain could lead RANS equations to finally converge to the correct mean flow field.

In the following subsections, the discussions are focused on the aforementioned two challenges, along with relevant preliminary solutions used in this computational framework. The effective form of the Reynolds stress tensor is discussed in Sec. 2.2, and the initial solution to build a one-to-one mapping relation for ML models are shown in Sec. 2.3.

2.2. Effective Form of the RANS Closure Term

The objective of this section is to present an optimal way to incorporate an expression equivalent to the high-fidelity Reynolds stress tensor, $\boldsymbol{\tau}_h$, into the RANS equations in order to compute a solution in close proximity to the high-fidelity mean flow field (\mathbf{u}_h, p_h) . The

solution of the RANS equations should be very close to the high-fidelity mean flow field (\mathbf{u}_h, p_h) if the high-fidelity Reynolds stress field $\boldsymbol{\tau}_h$ is mapped into the flow domain. However, Wu *et al.* [37] have reported that using an explicit form for the statistically averaged Reynolds stress tensor as a source term in the RANS equations does not naturally guarantee a correct *a posteriori* solution for the mean velocity and pressure field. The RANS equations commonly used in steady-state incompressible solvers, shown in Eq. (2), would face an ill-conditioned problem when the Reynolds stress tensor field is directly added to the right-hand side as part of the equation

$$(\mathbf{u}^{n-1} \cdot \nabla - \nabla \cdot \nu \nabla) \mathbf{u}^n = -\nabla p^{n-1} + \nabla \cdot \boldsymbol{\tau}^{n-1} + \mathbf{f}^{n-1}, \quad (2)$$

in which, the left hand side of the equation $\mathcal{L}(\cdot) = (\mathbf{u}^{n-1} \cdot \nabla - \nabla \cdot \nu \nabla)$ is treated implicitly as the linear operator on the unknown, \mathbf{u}^n . And the right hand side $-\nabla p^{n-1} + \nabla \cdot \boldsymbol{\tau}^{n-1} + \mathbf{f}^{n-1}$ is treated explicitly as known variables from the previous iteration step.

If the high-fidelity mean flow fields are interpolated into the flow domain with $(\mathbf{u}^{n-1}, p^{n-1}) = (\mathbf{u}_h, p_h)$ and $\boldsymbol{\tau}^{n-1} = \boldsymbol{\tau}_h$, the expected solution should be $(\mathbf{u}^n, p^n) \approx (\mathbf{u}_h, p_h)$. But with the problem being ill-conditioned, the error in the solution $\|\delta \mathbf{u}^n\|$ is extremely sensitive to the statistical errors in the closure $\|\nabla \cdot \delta \boldsymbol{\tau}^{n-1}\|$. Results of existing research focusing on channel flows have shown that the velocity field at steady-state would deviate from the high-fidelity solution by over 35% at a high Reynolds number [40], and similarly, identical Reynolds stress fields obtained from different data sources could result in vastly different solutions in terms of mean velocity [37]. To circumvent the issue yielded by the explicit approach not being suitable, Wu *et al.* [37] have proposed to compute the eddy-viscosity field from the high-fidelity database and interpolate it into the flow domain as part of the left-hand side of the equation, which could improve the conditioning of the linearized momentum equation. To achieve this goal, the closure $\boldsymbol{\tau}$ is decomposed into a linear and a non-linear part, shown in Eq. (3)

$$\boldsymbol{\tau} = 2\nu_t \mathbf{S} + \boldsymbol{\tau}_\perp \quad (3)$$

$$\boldsymbol{\tau} = \nu_t \nabla \mathbf{u}^n + \nu_t \nabla^T \mathbf{u}^{n-1} + \boldsymbol{\tau}_\perp^{n-1} \quad (4)$$

With the implicit part passed to the left-hand side (Eq. (4)), the linearized momentum equation with improved conditioning reads

$$(\mathbf{u}^{n-1} \cdot \nabla - \nabla \cdot (\nu + \nu_t) \nabla) \mathbf{u}^n = -\nabla p^{n-1} + \nabla \cdot \boldsymbol{\tau}_\perp^{n-1} + \mathbf{f}^{n-1} + \nabla \cdot \nu_t \nabla^T \mathbf{u}^{n-1} \quad (5)$$

Because of the better-conditioned momentum equation obtained by the implicit treatment of the linear part, small errors in the eddy-viscosity closure will not be amplified and propagated to the solution, and the solution of the new equations can be very close to the mean flow of the high-fidelity simulations.

Currently, the estimation of the optimal eddy-viscosity is computed by minimizing the discrepancy between the linear part of the stress and the DNS Reynolds stress data, shown in Eq. (6).

$$\nu_t^m = \arg \min_{\nu_t} \|\boldsymbol{\tau}_h - 2\nu_t \mathbf{S}_h\| \quad (6)$$

$$\nu_t^m = \left| \frac{\tau_{h_{ij}} S_{h_{ij}}}{2 S_{h_{ij}} S_{h_{ij}}} \right| \quad (7)$$

Eq. (7) illustrates the point-wise least square approximation to estimate eddy-viscosity from the high-fidelity database. It should be mentioned that this estimation might encounter numerical discontinuity where the misalignment of the principal axis of \mathbf{S}_h and $\boldsymbol{\tau}_h$ changes rapidly, for example, at the boundary of the re-circulation zone in a flow with separation. For this reason, the universal solution to for the estimation of ν_t from high-fidelity database still needs to be further investigated.

In the present study, the turbulent channel flow is taken as an example to illustrate the overall process of the computational framework and adopt Eq. (7) to process eddy-viscosity from DNS databases. Note that in the case of the planar channel flow with homogeneous streamwise and spanwise directions, only the Reynolds shear stress, τ_{12} , has a contribution to the RANS equation (Eq. (1)). Therefore, the linear part of the Reynolds stress could give the totally equivalent effect to the momentum equations, so the eddy-viscosity, ν_t , becomes the only term that needs to be modeled under this type of flow. In the presented study, the normalized eddy-viscosity, $\nu_t^* = \nu_t^m / \nu$, is taken as the learning target for the ML regression model, and the improved conditioning equations could ensure that if a correct eddy-viscosity field is predicted by the ML model, the RANS solver will return a correct mean velocity.

2.3. Constructing a Proper ML Regression System based on the Constitutive Theory

First order RANS turbulence models are built from a constitutive relation between the Reynolds stresses and the velocity gradients. The simplest one are based on the Boussinesq approximation while the most general form is proposed by Pope [26]. This constitutive relation relies on a basic fundamental assumption, which is that the normalized deviatoric tensor of Reynolds stress, \mathbf{b}^* , is a function of the normalized strain and rotation tensors, \mathbf{S}^* and $\boldsymbol{\Omega}^*$, as presented in Eq. (7).

$$\mathbf{b}^* = \mathbf{f}(\mathbf{S}^*, \boldsymbol{\Omega}^*), \quad (8)$$

in which, the normalized deviatoric tensor of Reynolds stress is $\mathbf{b}^* = \frac{\boldsymbol{\tau}}{k} - \frac{2}{3} \mathbf{E}$, where \mathbf{E} is the identity matrix and k is the turbulence kinetic energy. The normalized strain and rotation tensor are respectively defined as $\mathbf{S}^* = \frac{1}{2} \frac{k}{\epsilon} (\nabla \mathbf{u} + \nabla^T \mathbf{u})$, $\boldsymbol{\Omega}^* = \frac{1}{2} \frac{k}{\epsilon} (\nabla \mathbf{u} - \nabla^T \mathbf{u})$, where ϵ is the dissipation rate of turbulence kinetic energy.

Under the tensor analysis theory (i.e., the Cayley-Hamilton theorem [27]) and the matrix polynomial expansion [28, 29], Eq. (8) is actually equivalent to a finite linear combination of integrity tensor bases, which can be written as

$$\mathbf{b}^* = \sum_{m=1}^{10} G^{(m)} \mathbf{T}^{(m)} \quad (9)$$

where $G^{(m)}$ is the combination coefficient of tensor base $\mathbf{T}^{(m)}$. The full expression of the tensor bases $\mathbf{T}^{(m)}$, can be found in Appendix A. Under this mathematical expression, the modeling task can be simplified to the functional mapping between combination coefficients and tensor invariances

$$G^{(m)} = g^{(m)}(\lambda_1, \dots, \lambda_5) \quad (10)$$

where λ_l ($l = 1$ to 5) is defined as follows:

$$\lambda_1 = \text{tr}(\mathbf{S}^{*2}), \lambda_2 = \text{tr}(\mathbf{\Omega}^{*2}), \lambda_3 = \text{tr}(\mathbf{S}^{*3}), \lambda_4 = \text{tr}(\mathbf{\Omega}^{*2}\mathbf{S}^*), \lambda_5 = \text{tr}(\mathbf{\Omega}^{*2}\mathbf{S}^{*2}) \quad (11)$$

and tr is the trace of the tensors.

The existing turbulence constitutive relations can be treated as the truncated form of Eq. (9). For example, the linear eddy-viscosity model (i.e., the Boussinesq hypothesis) is based on the first term of Eq. (9), whereas the quadratic eddy-viscosity model [41] keeps $\mathbf{T}^{(1-4)}$ for a better approximation.

However, one significant problem in the basic assumption of this constitutive relations (Eq. 8) is that the independent variables (i.e., \mathbf{S}^* and $\mathbf{\Omega}^*$) are not capable of determining the function value of \mathbf{b}^* from the DNS data. That is to say, even the most advanced form of the existing constitutive relations is a multi-valued function, where the function value, \mathbf{b}^* , might return very different answers even if the same independent variables, \mathbf{S}^* and $\mathbf{\Omega}^*$ are used as input data.

To explain the previous argument, the pattern of how \mathbf{b}^* changes with \mathbf{S}^* and $\mathbf{\Omega}^*$ is looked at in a turbulent channel flow using the data of Abe *et al.* [42] at $Re_\tau = 180$ ($Re_\tau = \frac{u_\tau h}{\nu}$ with $u_\tau = \sqrt{\nu \frac{du}{dy}}$ and h is the half height of channel). The statistical averaged quantities in DNS channel case only have one degree of freedom which changes along the wall-normal direction. Both \mathbf{S}^* and $\mathbf{\Omega}^*$ are solely determined by $\frac{k}{\epsilon} \frac{\partial u}{\partial y}$, as all the other components are nil. The constitutive relation can be visualized in Fig. 3, with $S_{12}^* = \Omega_{12}^* = \frac{1}{2} \frac{k}{\epsilon} \frac{\partial u}{\partial y}$ in the x -axis and $b_{12}^* = \frac{\tau_{12}}{k}$, the only effective component of the momentum equations, normalized by the turbulent kinetic energy in the y -axis.

Figure 3 shows that the constitutive relation determined by \mathbf{S}^* (resp. $\mathbf{\Omega}^*$) is not a single-valued function. For example, given the same input value (e.g., $S_{12}^* = 4$ in Fig. 3), the DNS data returns two different function values ($b_{12}^* \approx 0.15$ in the outer layer and $b_{12}^* \approx 0.05$ in the inner layer). Treating any one of these two values as noise and filtering it out would be inappropriate because all the different branches of the data have clear physical meanings. However, for most deterministic ML algorithms (e.g., artificial neural network), the algorithms are designed under the principal premise that the input-output is a one-to-one mapping relation [43, 44]. Handling such a multi-valued function would make the ML regression model struggle to minimize the mean square error for the training data. Considering the example of two data points located on different branches, namely $P_1(x_0, y_1)$ and $P_2(x_0 + \delta x, y_2)$, but where their abscissa only differs by a tiny number δx , the very

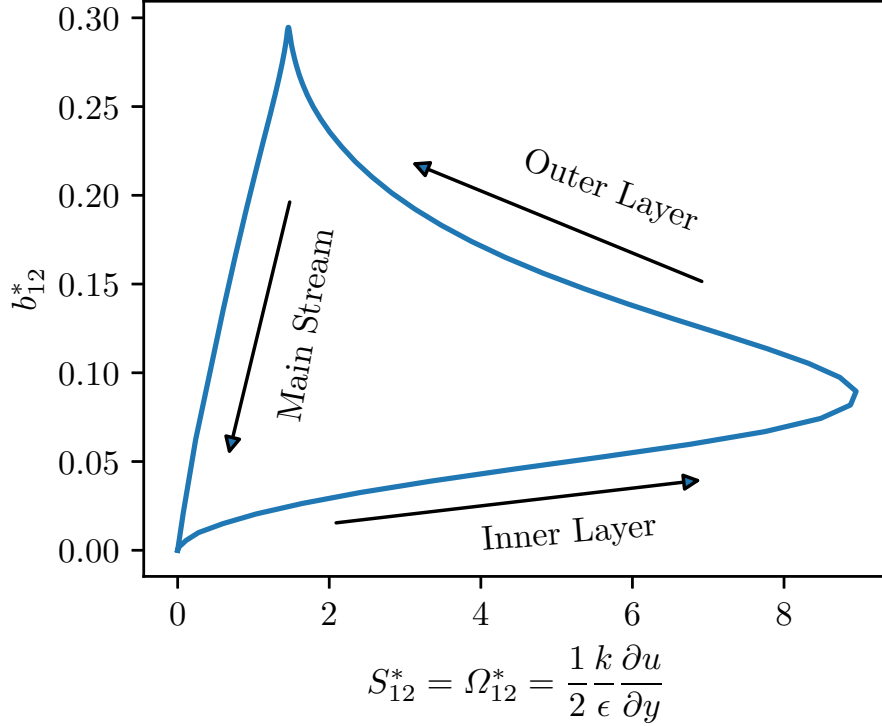


Figure 3: Constitutive relation in turbulent channel flow

different output data would lead the ML models to face a tremendous increase from y_1 to y_2 inside the tiny $[x_0, x_0 + \delta x]$ interval, leading to large oscillations occurring in the machine-learned mappings [45], and affecting the differentiability and stability of the PDE system. Even if the model is perfectly regularized, the mean values between the different branches are returned to the RANS solver, and considerable structural uncertainties are thus brought into the PDE system.

To avoid the aforementioned issue and treat the problem as multi-valued, the set of independent variables needs to be expanded. This leads to building a proper regression system for ML algorithms. The advantage of the tensorial combination form (Eq. 9) is that the Reynolds stress tensor changes accordingly with the tensor bases $\mathbf{T}^{(m)}$ without changing the coefficients $G^{(m)}$. Therefore, such a mathematical form is independent from any rotational transform of the frame of reference, and adding more rotational invariant scalars q_j to the set of independent variables for the coefficients $G^{(m)}$ does not change the tensorial expressions. Besides, in order to ensure that the model does not depend on any specific types of flow, the extra scalars q_j should be defined as a dimensionless combination of local flow variables (e.g., k , ϵ , etc) rather than macro quantities (e.g., mass flow rate, Reynolds number, angle of attack, etc). And the functional form of $G^{(m)}$ becomes:

$$G^{(m)} = g^{(m)}(\lambda_1, \dots, \lambda_5, q_1, q_2, \dots) \quad (12)$$

Moreover, the aim of this work is to obtain a functional expression for the dimensionless

eddy-viscosity, in order to overcome the ill-conditioned problem identified in Sec. 2.2. By replacing the dimensional definition into Eq. (9) with $\mathbf{S} = \frac{k}{\epsilon} \cdot \mathbf{S}^*$, $\boldsymbol{\tau} = k \cdot (\mathbf{b}^* + \frac{2}{3}\mathbf{E})$, the dimensional form of the constitutive equation reads:

$$\boldsymbol{\tau} = \frac{k^2}{\epsilon} (G^{(1)} \mathbf{S}) + k \sum_{m=2}^{10} G^{(m)} \mathbf{T}^{(m)} + \frac{2}{3} k \mathbf{E} \quad (13)$$

$$= 2\nu_t \mathbf{S} + \boldsymbol{\tau}^\perp \quad (3)$$

Comparing Eq. (13) with the decomposition in Eq. (3), the coefficient of the linear term defines the functional form of the eddy-viscosity, which gives:

$$\nu_t = \frac{1}{2} \frac{k^2}{\epsilon} G^{(1)} \quad (14)$$

For example the original k - ϵ model [4] gives $\nu_t = C_\mu \frac{k^2}{\epsilon}$ as a special constant function for $G^{(1)}$. From Eq. (14), one could derive that the dimensionless eddy-viscosity $\nu_t^* = \frac{\nu_t}{\nu}$, which is the learning target inside this study, and can be written as:

$$\nu_t^* = \frac{\nu_t}{\nu} = \frac{1}{2} \frac{k^2}{\nu \epsilon} G^{(1)} = f(\lambda_1, \dots, \lambda_5, q_1, q_2, \dots, \frac{k^2}{\nu \epsilon}) \quad (15)$$

Equation (15) shows that the eddy-viscosity depends on the dimensionless coefficient $G^{(1)}$ and a special normalization factor $\frac{k^2}{\nu \epsilon}$, which is the ratio between the eddy-viscosity predicted by traditional RANS models, $\frac{k^2}{\epsilon}$, and the molecular viscosity, ν . Because this factor is coordinate-transformation invariant, it can be included in the additional set of independent variables \mathbf{q} .

According to our experience in the actual practice, the ML model trained with $\boldsymbol{\lambda}$ in the functional definition of ν_t^* would cause a numerical instability during the iteration process. Therefore, the final functional form for the ML task can be written as:

$$\nu_t^* = f(q_1, q_2, \dots) \quad (16)$$

where the special factor $\frac{k^2}{\nu \epsilon}$ must be included in the set $\{q_1, q_2, \dots\}$. In this way, the multi-valued problem can be avoided in the ML regression system, because enough independent variables for the determination of the local eddy-viscosity are used.

In this work, the conventional SST k - ω model [6] is adopted because of its numerical stability and integrability in the near-wall region. Yet the production of k and ω shares the same dimension with ϵ , so it is thus equivalent to $\epsilon = \frac{k}{\omega}$. The dimensionless scalar becomes

$\frac{k}{\nu\omega}$, via the substitution of ϵ . And the full list of the additional independent set of \mathbf{q} can be found in Table. 1, along with their physical meanings and the adjustment to have a relatively uniform range for the input features.

Table 1: List of non-dimensional input features for ML model

Variable	Description	Definition	Normalization	Actual input
q_1	Turbulence intensity	k	$\frac{1}{2}U_iU_i$	$\frac{25k}{25k + 0.5U_iU_i}$
q_2	Normalized factor	$\frac{k}{\nu\omega}$	Not applicable ^c	$\frac{k}{50\nu\omega}$
q_3	Wall distance	d^*	$\frac{\nu}{\sqrt{k}}$	$\frac{\sqrt{k}d}{50\nu}$
q_4	Cross diffusion of k and ω	$\frac{\partial k}{\partial x_i} \frac{\partial \omega}{\partial x_i}$	ω^3	$10 \left(\frac{1 + 680\chi_k^2}{1 + 400\chi_k^2} - 1 \right)^{**}$
q_5	Variables in SST model to characterize	$\frac{\sqrt{k}}{\omega d}$	Not applicable	$\frac{5\sqrt{k}}{\omega d}$
q_6	viscous sublayer and turbulent region	$\frac{\nu}{\omega d^2}$	Not applicable	$\frac{200\nu}{\omega d^2}$

^c Not applicable means the normalization is not necessary.

^{*} d is the distance to the wall.

^{**} $\chi_k = \max \left(\frac{1}{\omega^3} \frac{\partial k}{\partial x_i} \frac{\partial \omega}{\partial x_i}, 0 \right)$

2.4. Summary of Methodology and Numerical Platform

To sum up, with the aim that the RANS solver could reproduce the mean flow results of high-fidelity simulations, the training stage of the ML-RANS framework introduces conventional turbulence transport equations to process the high-fidelity mean flow, which ensures a consistent procedure to calculate the input features in the predicting stage (Sec. 2.1). Furthermore, the decomposition of the Reynolds stress and the implicit treatment of the RANS equations ensures that they do not amplify the statistical errors present in the closure term so that a well-predicted closure term can lead the RANS solver to converge to the correct results (Sec. 2.2). However, the previously defined constitutive relation exhibits a multi-valued problem when results are compared to DNS data, which proves difficult to be solved by ML algorithms. Here the set of independent variables is expanded to construct a one-to-one mapping in order to build a proper regression system for ML algorithms (Sec. 2.3). With the initial solutions in Sec. 2.2 and Sec. 2.3, the computational steps corresponding to Circles 2 and 3 in Fig. 2 can be fulfilled so that the computational framework can thus own a built-in solution which is the same as high-fidelity mean flows.

As for the numerical platform for CFD, the preparation of the training data refers to interpolating the high-fidelity mean flow field onto a RANS-designed mesh and running the traditional turbulence transport equations as scalar transport equations. This part is programmed in the Finite-Volume open-source CFD code OpenFOAM [46]. The improved conditioning RANS equations (Eq. 4) for the prediction phase are also implemented with the SIMPLE [39, 47] algorithm to deal with pressure-velocity coupling problem.

For the training of the ML models, Google’s Tensorflow [48] machine learning framework is adopted for its convenient construction of the artificial neural network and the most abundant application programming interface (API) support in major programming languages among other ML frameworks [48, 49, 50, 51]. The turbulence quantities are extracted from the scalar transport equations, along with the mean flow variables to assemble the input features (Table. 1). The neural network is trained independently and loaded through a self-developed Tensorflow-OpenFOAM-Interface (TOI) [52], where the interface feeds the current flow field as inputs to the ML model, and receives the output from the Tensorflow library.

Based on the discussions above, the calculation process is summarized as follows:

1. The accurate mean flow field is provided by a DNS, based on which the transport equations of k and ω , for the k - ω SST turbulence model are solved.
2. The input features for the ML model, $\{q_j\}$, are constructed as function of the mean velocity and turbulent quantities as shown in Table 1.
3. The learning target (i.e., the accurate eddy-viscosity) for the ML model is obtained from the DNS data by calculating ν_t using Eq. (7).
4. The mapping between $\{q_j\}$ and the eddy-viscosity is stored in the ML model after the training stage.
5. The OpenFOAM RANS solver computes the input features based on the current (initial) mean velocity and pressure field.
6. The ML model receives the current inputs and returns the eddy-viscosity field to the RANS solver through TOI.
7. The RANS solver receives the eddy-viscosity from the ML model and computes the corresponding velocity field, using Eq. (5).
8. The process is repeated from Step 5 to Step 7 until the residual reaches the convergence criteria.

3. Results and Discussion

In this section, an artificial neural network with continuous activation function is trained using the DNS data from planar turbulent channel flows at low to moderate Reynolds numbers. The DNS data from Abe *et al.* [42] and Moser *et al.* [53] (the latter is known as the KMM database) are used as the training and validation datasets, respectively. In the training process, the training data are used by the optimization algorithms to adjust weights in ANN, whereas the validation data are used to monitor and control the training process by adjusting the hyperparameters such as the structure of ANN and learning rate. The

newly developed ML-RANS model is firstly tested in turbulent channel flows at the same Reynolds number with the training data to verify the reproducibility of the training cases, and at Reynolds numbers equally distributed within the range of training data to assess the interpolation capability. A further test in flow over periodic hills [54] is also performed to validate the prediction capability in a flow regime that deviates from the training cases. Details of the training dataset and test cases are given in Table. 2.

Table 2: List of training dataset and testing dataset

Training Phase		Prediction phase		
Training set	Validation set	Test case		
Planar channel [42]	Planar channel [53]	Planar channel	Periodic hills	
$Re_\tau = 180^a$	$Re_\tau = 587.1$	$Re_\tau = Re_\tau^{train}, Re_\tau^{valid}$	$Re_h = 1400^b$	
$Re_\tau = 395$		$Re_\tau = 180, 230, \dots, 630$		
$Re_\tau = 640$				

^a Re_τ is the Reynolds number based on the mean wall fiction velocity and the half-height of a channel.

^b Re_h is the Reynolds number based on the bulk velocity and the height of the hill.

3.1. Training Phase

There are six raw input variables for the ANN, $q_1 - q_6$, as listed in Table 1, and the output data is the dimensionless eddy-viscosity calculated by Eq. (7) and normalized by the molecular viscosity ν .

The variation of the input profiles q_n as functions of the wall distance is shown in Fig. 4. Note that the intrinsic degree of freedom in this regression system is **two** because any variable in the flow can be uniquely determined by the dimensionless distance to the wall, y^+ , and Reynolds number of the flow. Fig. 4 shows four different patterns for the input parameters $\{q_n\}$. Therefore, the degree of freedom of input feature is larger than the degree of freedom of the regression system, so that a one-to-one mapping relation can be easily established through the ML algorithm. Moreover, we can also observe the similar distributions between q_2 and q_3 , and between q_1 and q_6 as well. This indicates the six input variables are redundant for the regression system. Consequently, regularization techniques are needed to eliminate the multicollinearity. In this work, the L1 regularization strategy [55] is adopted, which shrinks the weight of the ANN layers to zero to achieve a better generalization capability. The total loss of the ANN is defined as

$$Loss = \sum_{k=1}^N (f(x_k) - y_k)^2 + \lambda \sum_{i,j}^{m,n} |\omega_{ij}| \quad (17)$$

where N is the number of the data point, m and n are the numbers of layers and nodes in the ANN, respectively. The optimization is applied to both parts of the loss. The first part is the mean square error (MSE) from the training data, and the second part is the

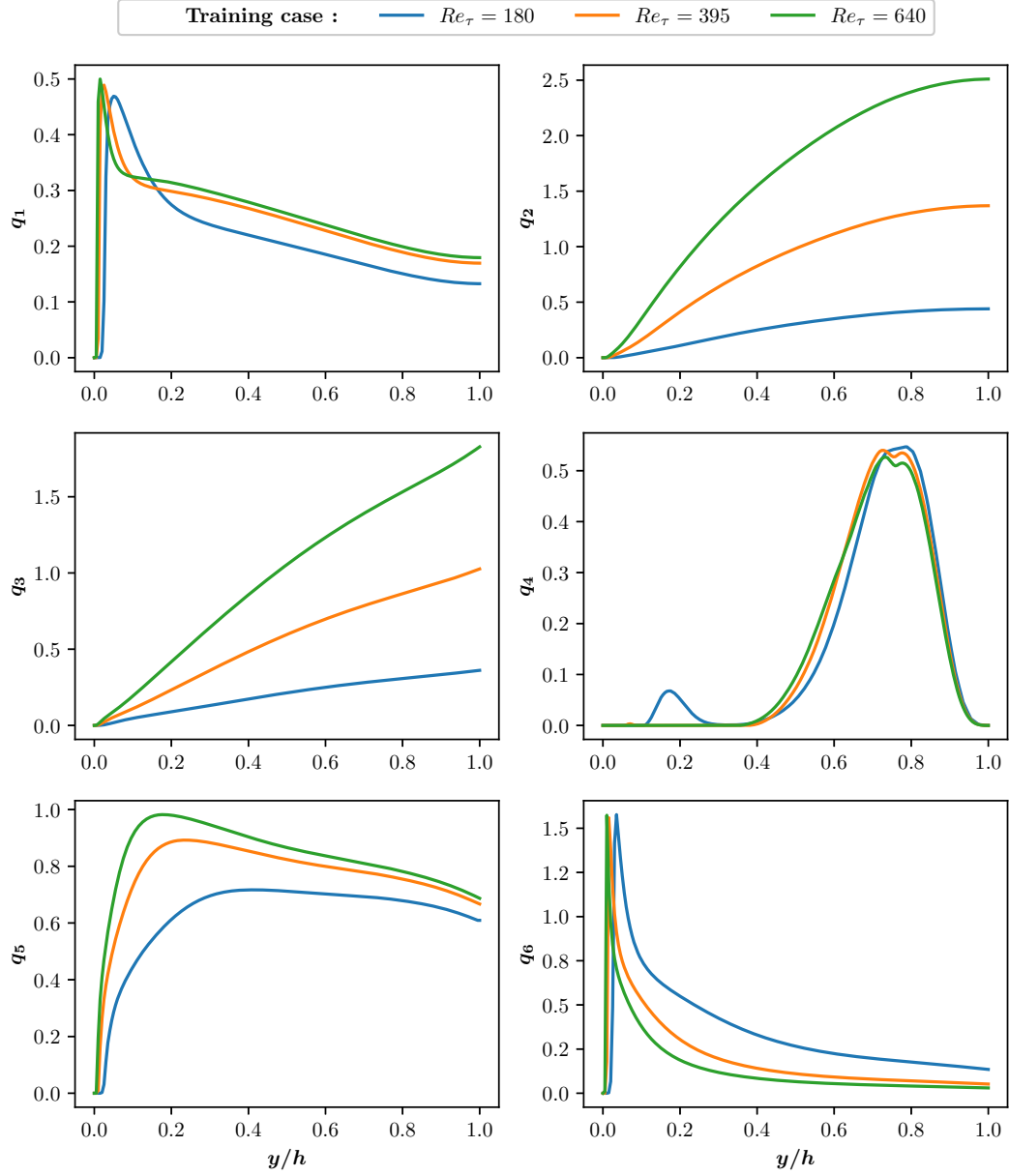


Figure 4: Profiles of the input variables of the ANN in channel flows

L1 regularization penalty, minimizing the weight of each layer [55]. The evolution of errors during the training process can be seen in Fig. 5.

In Fig. 5, the quality of the training dataset is observed better than the validation dataset in terms of the number of samples for averaging and the smoothness of the high-order statistics. Consequently, the magnitude of MSE of the validation data is larger than

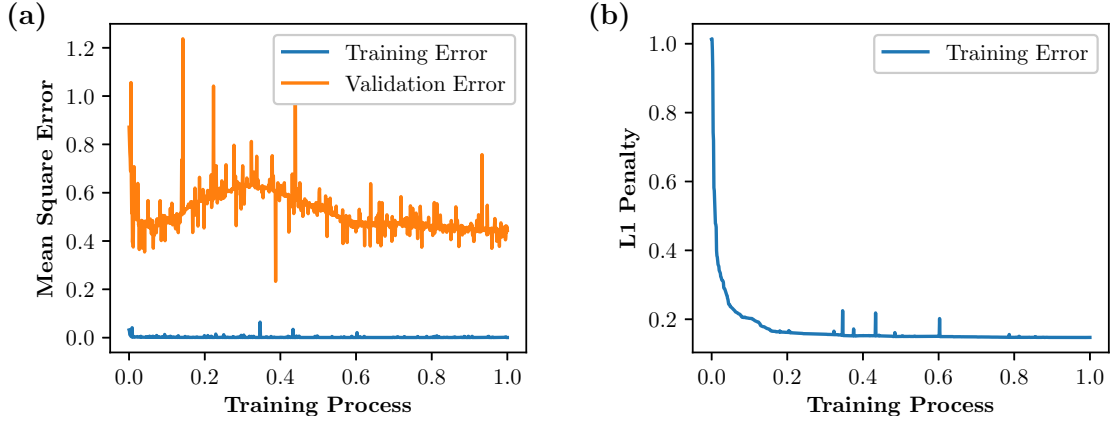


Figure 5: Losses in the training process. (a): MSE loss (b): L1 penalty term. The x -axis is defined as the ratio of current training step and total training steps.

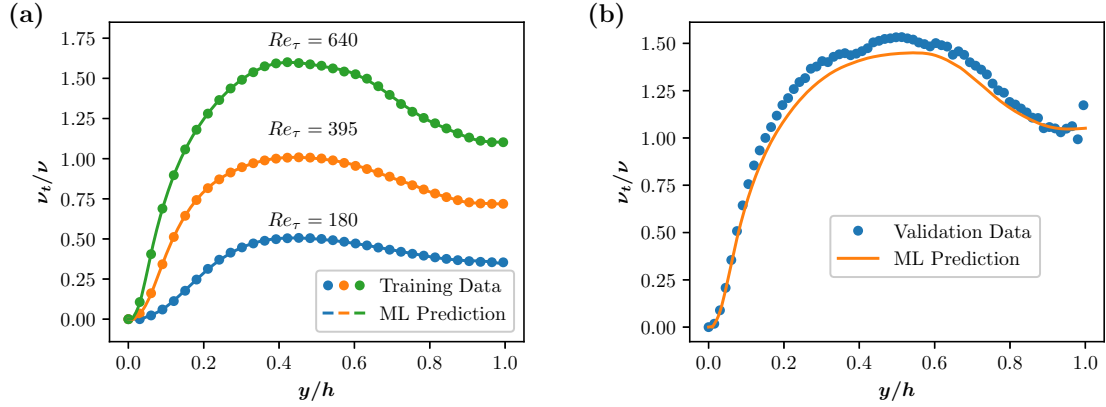


Figure 6: The eddy-viscosity fitted by the ANN at the end of the training phase. (a): Performance on the training set (b): Performance on the validation set

Table 3: Hyper parameters of a successful training of ANN

Hyper Parameters	Recommend Values
Number of Hidden Layers	3
Number of Nodes per Layer	24
Activation Function	tanh
Optimizer	Adam Optimizer
Learning Rate	0.002
L1 Regularization Coefficient	0.025
Epoch Numbers	1500000

that of the training data. But at the end of the training, the error of the validation data converges to the lowest level, indicating that the ML model is not over-fitted in the training process.

The *a priori* result of the eddy-viscosity is presented in Fig. 6. It can be seen that the eddy-viscosity is perfectly predicted in the training dataset, and a satisfactory result is achieved in the validation dataset as well.

During the training phase, the overfitting problem is avoided by using a set of noisy data to monitor and control the training process, leading to a satisfactory *a priori* prediction of both the training and the validation sets. The details of the hyperparameters in ANN are listed in Table 3.

3.2. A Posteriori Results in Test Cases

After the training stage, the weights of each layer in the ANN are frozen, and the ML model is ready for an online prediction. In the prediction phase, the ANN model saved in the frozen Tensorflow graph is loaded to the CFD solver to predict the eddy-viscosity at each iteration step based on the input features composed with the runtime flow field.

3.2.1. Planar Turbulent Channel Flows

The developed ML model is tested in turbulent channel flows, which is depicted in Fig. 7. The grid convergence study of the channel flow with both $k-\omega$ SST model and the ML model is shown in Fig. 8, from which we can observe a converged friction coefficients when y^+ in the first layer is less than 2, therefore the set of the mesh listed in Table 4 is adopted in the *a posteriori* cases with first point off the wall satisfying $y^+|_{wall} \approx 1$ and the maximal mesh resolution $\Delta y_{\max}^+ < 4$. The initial field for each test is the converged solution from $k-\omega$ SST model. The residuals of velocity and eddy-viscosity are monitored in Fig. 9.

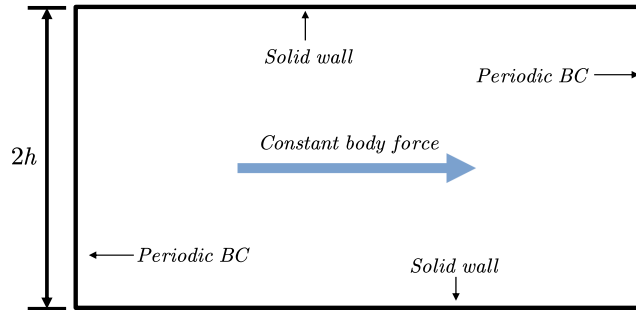


Figure 7: The geometry and boundary conditions for channel flow simulation

Table 4: Mesh details of RANS simulation

Reynolds Number (Re_τ)	Cell Number (wall normal)
$150 < Re_\tau < 300$	168
$300 < Re_\tau < 500$	372
$Re_\tau > 500$	558

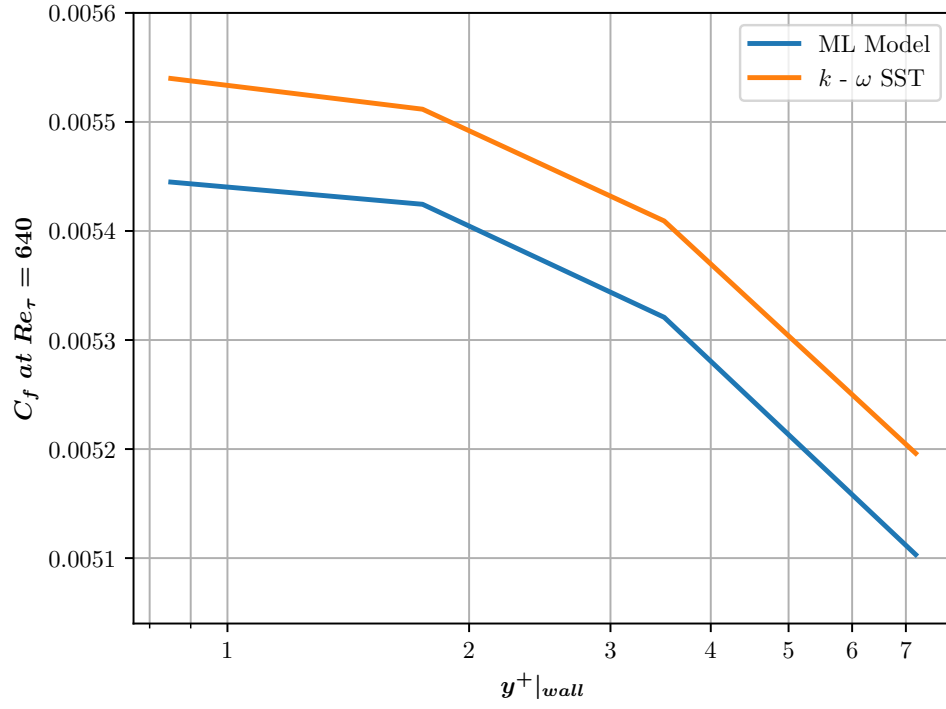


Figure 8: Grid convergence for channel flow at $Re_\tau = 640$

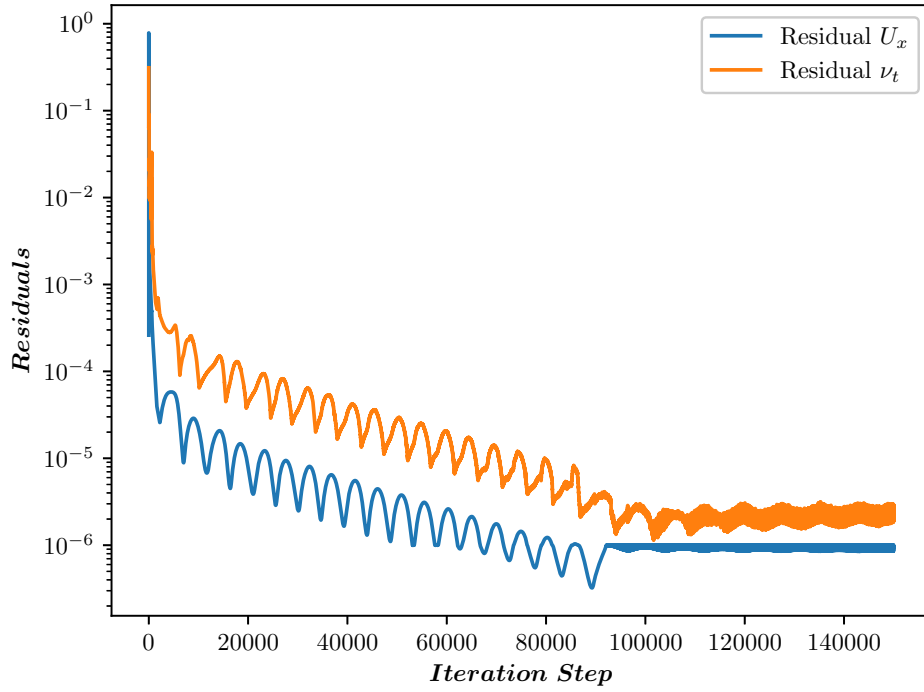


Figure 9: Evolution of residuals in the simulation of a channel flow.

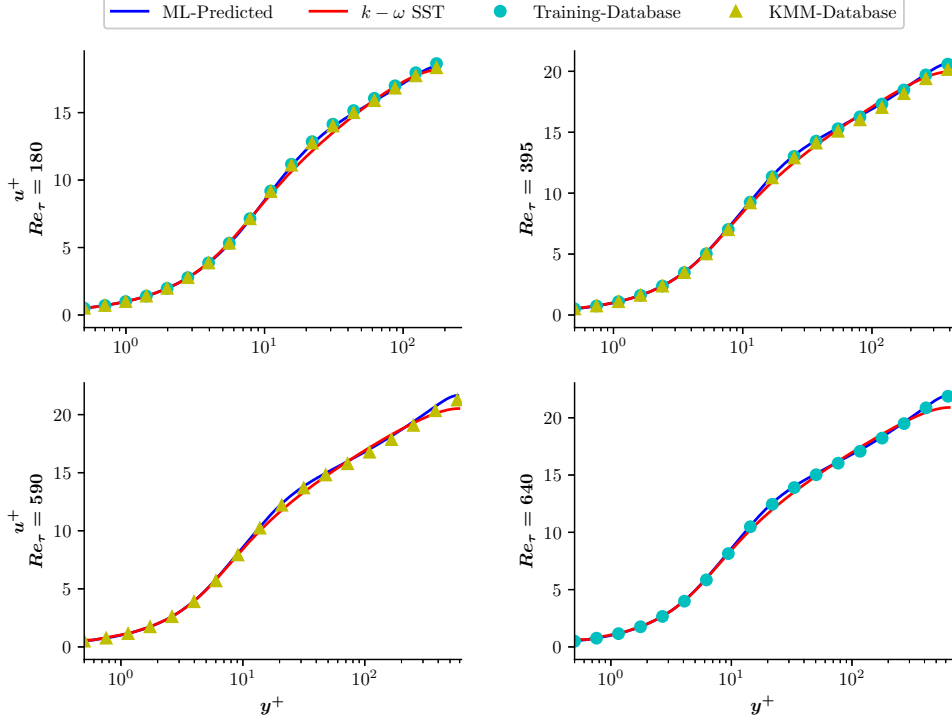


Figure 10: Comparison of velocity profile.

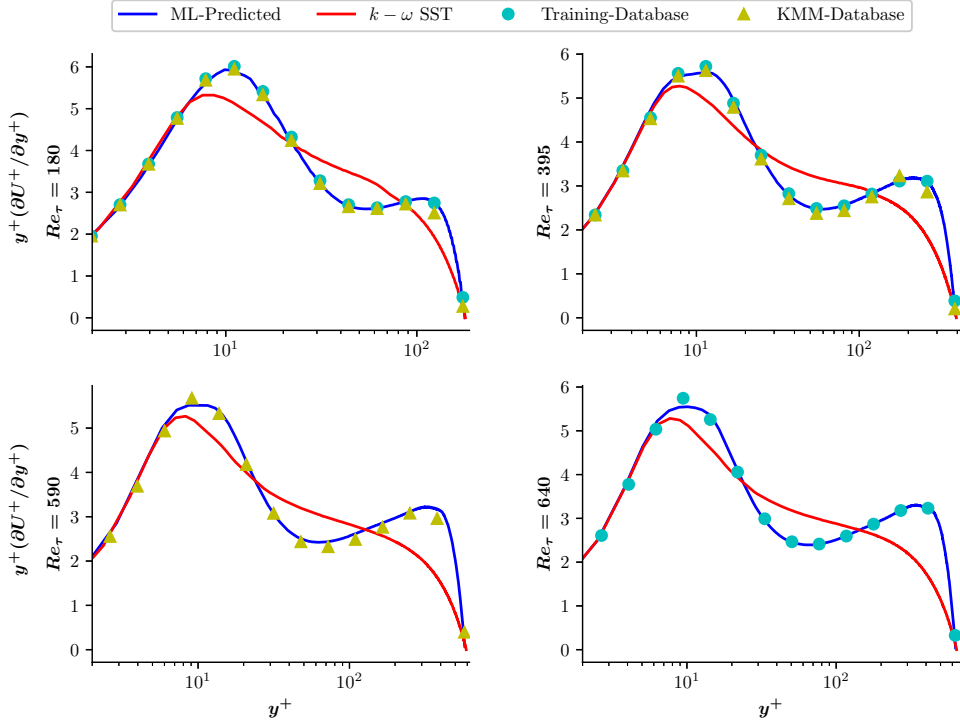


Figure 11: Comparison of $y^+(\partial U^+ / \partial y^+)$ distributions.

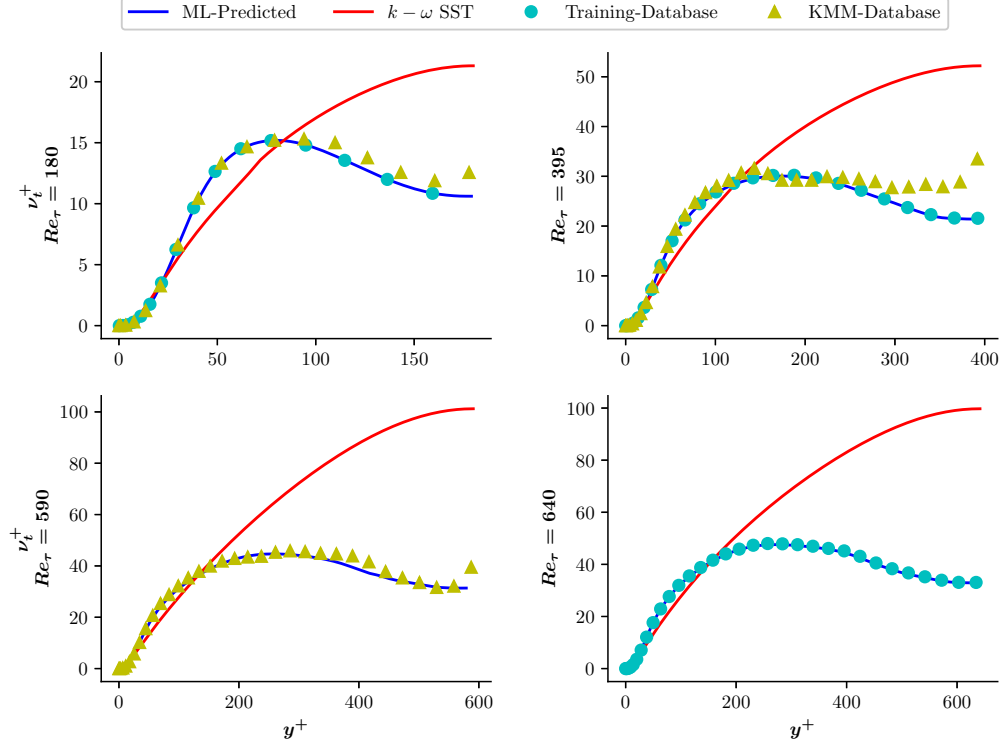


Figure 12: Comparison of eddy-viscosity distributions along wall normal direction.

The profiles of mean velocity and normalized mean velocity gradient, $y^+(\partial U^+/\partial y^+)$, from the *a posteriori* simulations are shown in Fig. 10 and Fig. 11 respectively. As expected, the mean velocity profiles are predicted accurately by the ML integrated turbulence model, with no noticeable difference with the DNS data. From the detailed comparison of velocity gradient profiles, we can further confirm that the traditional $k-\omega$ SST model failed to capture the peak and inflection points of the velocity gradient, and the present ML model presents a superior performance in predicting high-order statistics.

The eddy-viscosity profiles are compared in Fig. 12, from which we can see that the $k-\omega$ SST model shows an over-prediction of the eddy-viscosity in the most part of the channel, leading to errors in the prediction of mean velocity. The ML model improves the results significantly, and the profiles of eddy-viscosity for all cases agree well with the DNS data. The wiggles on the eddy-viscosity profiles of the KMM database might be due to the inadequacy of samples for averaging.

Besides, the analysis for quantitative errors is also performed under the definition of the root-mean-square error (RMSE) of streamwise velocity in channel flows, shown in Eq. (18).

And the RSME errors are compared in Table. 5

$$E = \frac{\sqrt{\frac{1}{Re_\tau} \int_0^{Re_\tau} (U_{dns}^+ - U_{rans}^+)^2 dy^+}}{\frac{1}{Re_\tau} \int_0^{Re_\tau} U_{dns}^+ dy^+} \quad (18)$$

Table 5: RSME errors compared with DNS at same Re_τ

Turbulence model	DNS Abe <i>et al.</i> [42]			KMM database [53]		
	$Re_\tau = 180$	$Re_\tau = 395$	$Re_\tau = 640$	$Re_\tau = 180$	$Re_\tau = 395$	$Re_\tau = 590$
$k-\omega$ SST	1.27%	1.74%	2.36%	1.26%	1.64%	2.13%
ML model	0.12%	0.08%	0.08%	0.29%	0.20%	0.26%

As Table. 5 shows, the ML model outperforms the conventional $k-\omega$ SST model with the error being an order of magnitude lower, indicating that a promising reproducibility of the training cases can be achieved in the present framework.

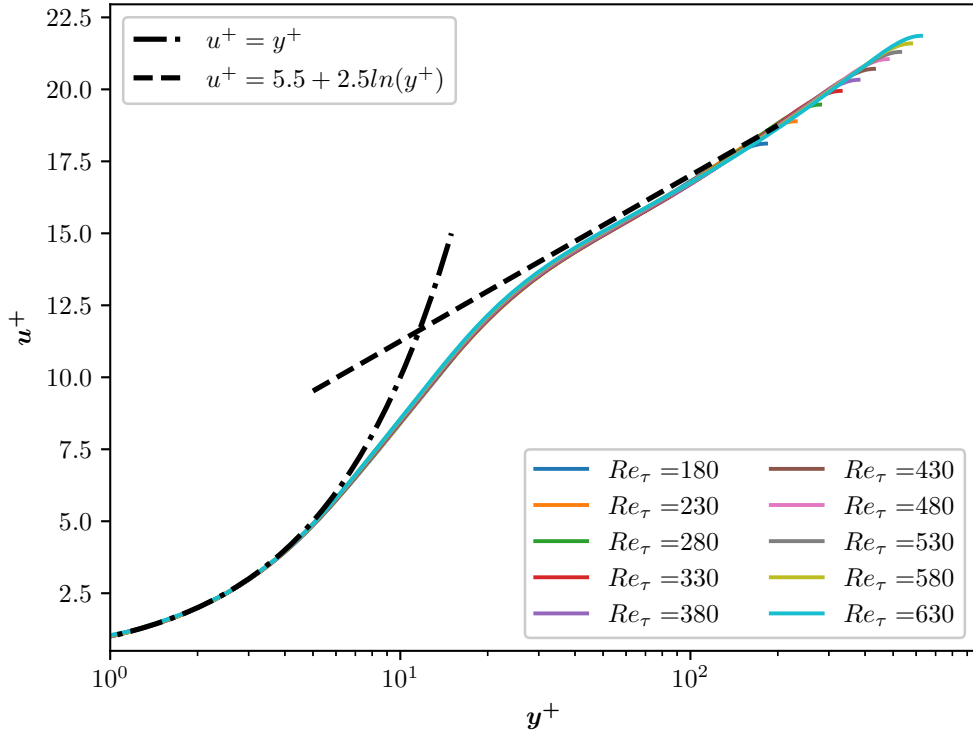


Figure 13: Mean velocity profiles in channel flows at equally spaced Reynolds numbers.

To further evaluate the robustness and interpolation capability of the developed ML model, we also test the ML-RANS model in the channel flow at Reynolds number changing

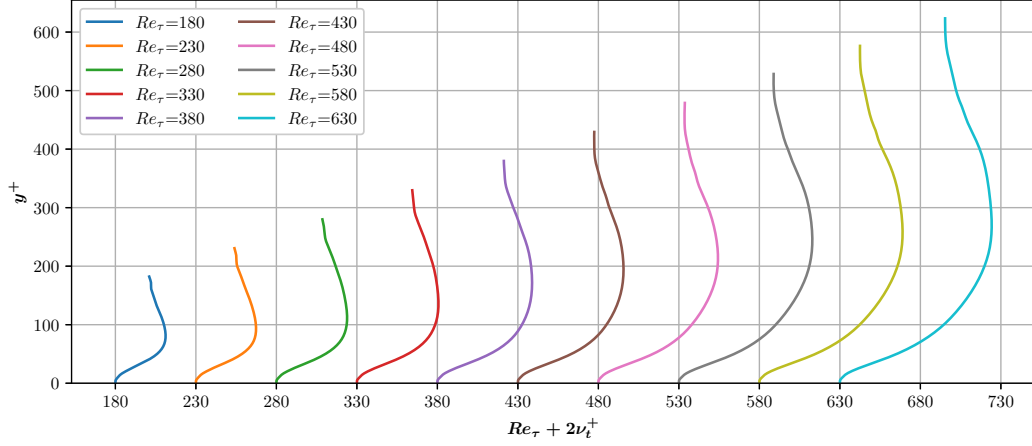


Figure 14: Distributions of eddy-viscosity in channel flows at equally spaced Reynolds numbers.

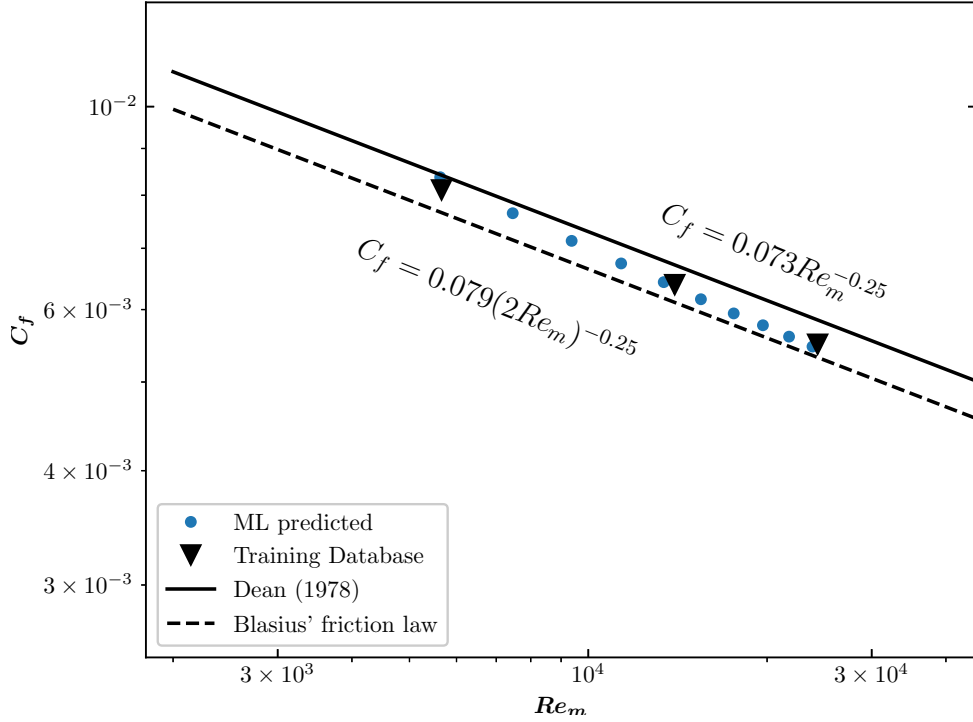


Figure 15: Comparison of friction coefficients of ML models prediction, DNS and analytical formula.

continuously from $Re_\tau = 180$ to $Re_\tau = 630$. The profiles of mean velocity and eddy-viscosity are presented in Fig. 13 and Fig. 14 respectively, and the skin friction coefficients are presented in Fig. 15. It can be confirmed that the linear law and the log law of the velocity profile are well preserved in all the tests, and the friction coefficients agree well with the law of Dean [56] and the Blasius friction law. From the results of this series of simulations, we can see a consistent changing of profiles with the Reynolds number, demonstrating favorable

robustness and interpolation capability of the ML model within the range of training data.

According to the *a posteriori* results, it can be confirmed that the developed ML-RANS framework can, not only obtain an iterative converged simulation, but also reproduce the mean flow field in the training cases. Besides, the ML-RANS framework can further perform a satisfactory interpolation capability at Reynolds number within the range of training data. Therefore, the reproducibility of training cases and a favorable interpolation capability can be achieved in the presented ML-RANS framework.

3.2.2. Flow over Periodic Hills

The ML-RANS model trained only with the data from channel flows can be applied to more complicated cases, since its input and output variables are all local-defined and independent with flow cases. Therefore, the flow over periodic hills at $Re_h = 1400$ is conducted to further examine the performance of the ML model. The geometry and boundary conditions are shown in Fig. 16, with the grid convergence verification shown in Fig. 17, and the 393×257 grid is adopted with the first layer of $y^+ \approx 0.12$ on the bottom wall.

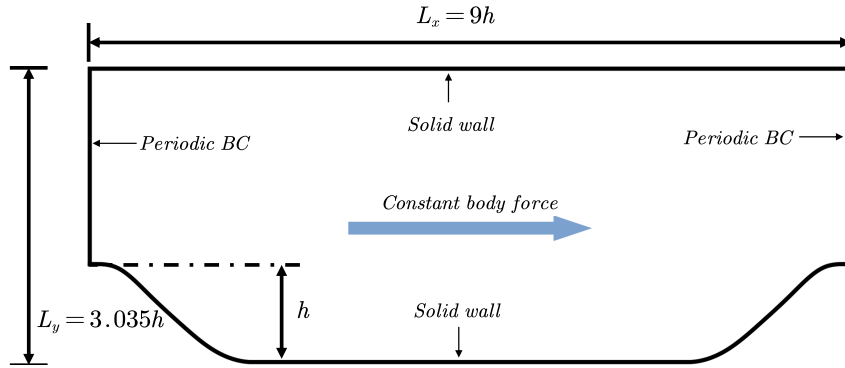


Figure 16: The geometry and boundary condition for channel flow simulation

Surprisingly, the ML model shows a clear improvement against the traditional model, even it is only trained with data from planar channel flows. The comparison of the mean velocity fields from DNS, $k-\omega$ SST model, and the ML model is presented in Fig. 19. The ML model presents a better result than the original $k-\omega$ SST model in terms of the size of the separation bubble and the location of the reattachment point. The comparison of mean skin friction and pressure coefficients on the bottom wall further proved the improved performance of the ML model, as shown in Fig. 18.

The uncertainty in the separated case might come from the isotropic nature of the solely usage of eddy-viscosity, failing to predict the condition where the principal axis of Reynolds stress tensor deviates from those of strain rate tensor. However, these results also show a great potential of the ML model to achieve a favorable prediction in complex flows, given enough training from simple cases. Besides, a trustful prediction is still available even the manifold of data from prediction cases is slightly different from the training sets.

Therefore, the ML model developed in the present study not only succeeds in the simulation of the same type of flow as the training case but also presents the potential in predicting

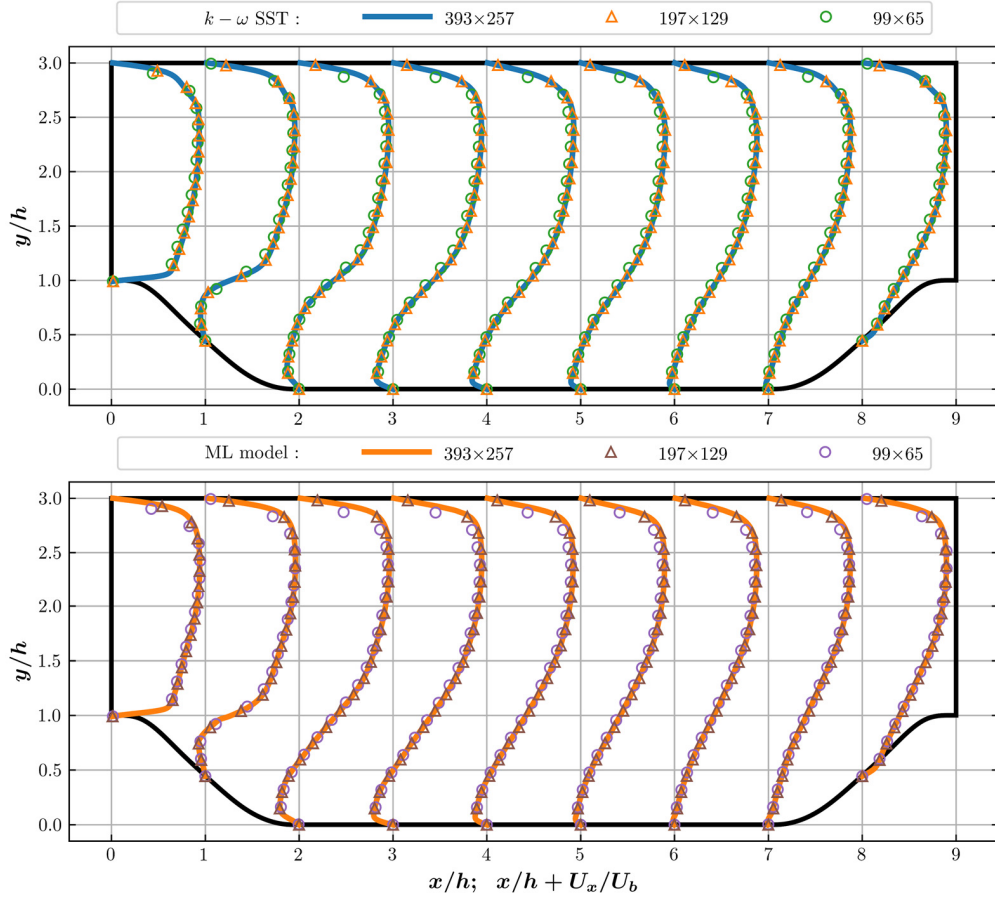


Figure 17: Stream-wise velocity profile in flow over periodic hills with different grid resolution.

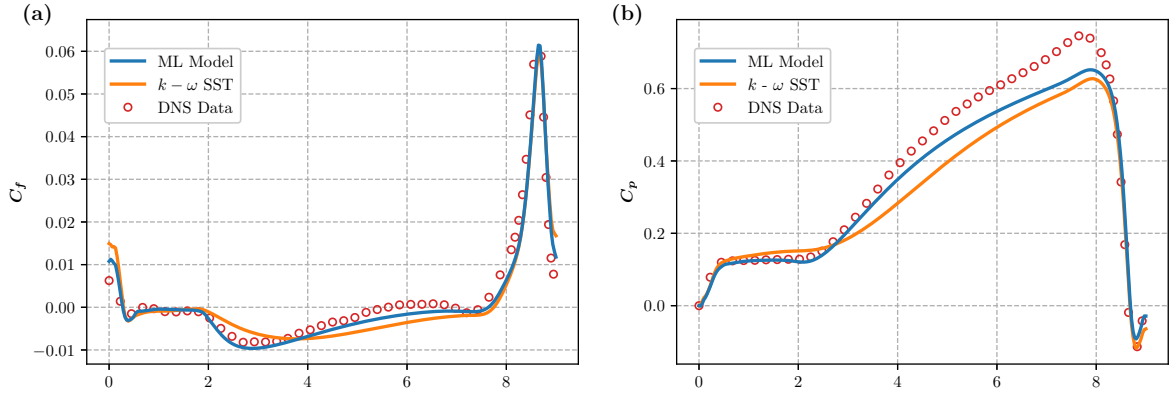


Figure 18: Distribution of friction coefficient (a) and pressure coefficient (b) on the bottom wall of the periodic hill.

a more complicated flow. This result is very encouraging for the further development and applications of the ML model.

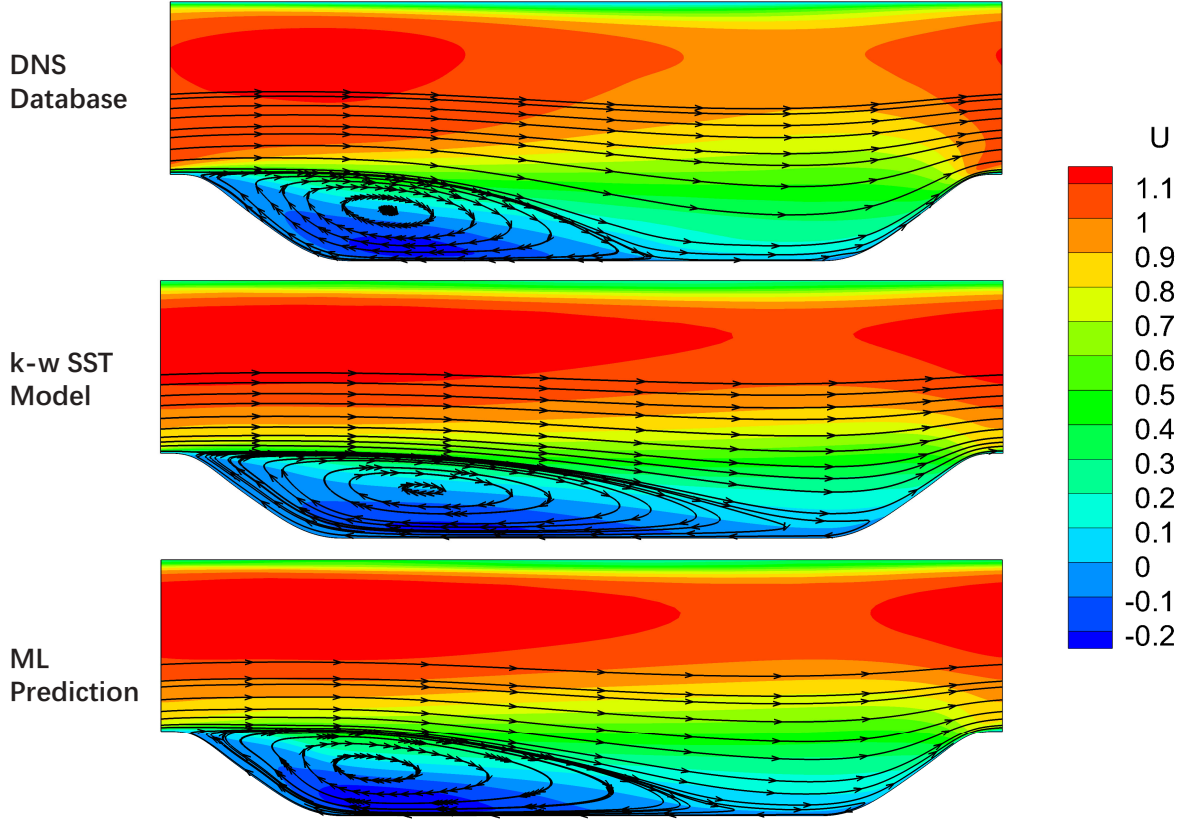


Figure 19: Mean velocity field in flow over periodic hills.

4. Conclusions - Perspectives

In this study, an iterative ML-RANS framework is developed aiming at a built-in reproducibility of the training cases. The following technical details are implemented into the computational framework to achieve this goal,

1. A conventional RANS model (the k - ω SST model is used for the present case) is incorporated in processing the training data so that the process of calculating input features in both the training phase and the predicting phase is ensured to be consistent. Also, this measure brings an empirical estimation for turbulence quantities into the system, making it possible to compose more independent variables for the ML regression system.
2. The Reynolds stress tensor is decomposed into the linear part and the residual nonlinear part, the linear part is treated implicitly and incorporated into diffusion terms in the RANS equations. This numerical strategy overcomes the ill-conditioning problem of RANS equations and ensures the correspondence between a correct closure term and a correct mean flow field.
3. The existing constitutive hypothesis is extended with more independent variables to ensure the sufficiency of the input feature of the ML model so that a single-valued

regression system suitable for ML algorithm can be thus established.

4. A program interface is developed to link the machine learning library to a CFD solver, and an iterative convergence is achieved in the *a posteriori* simulations.

Besides, the developed ML-RANS framework is trained under a cross-case strategy, with DNS data from the turbulent channel flows at $Re_\tau = 180, 395$, and 640 merged together to feed the ML model. The framework is tested in channel flows at Reynolds numbers equally spaced within the training range and the flow over periodic hills, and the results show the reproducibility of the training cases are successfully achieved. Apart from this, the ML model can also perform a favourable interpolation capability within the range of training data. For the test case in the flow over periodic hills, the ML model also outperforms the $k-\omega$ SST model, although the model has not been informed with any prior information about the non-equilibrium flow. The predicting capability indicates the promising potential of the current ML-RANS framework.

In spite of the $k-\omega$ SST model being incorporated in the current study, the current framework also has the potential to be developed by incorporating other turbulence models. Turbulence quantities from different empirical models can also be used simultaneously for one prediction despite the different physical intention behind those versions of models. In this sense, the developed ML-RANS framework can be regarded as the combination of the data-driven turbulence modeling and the traditional turbulence modeling, which can be expected to be further developed with better integration between the empirical knowledge and high-fidelity simulations.

Further developments are needed before the application of the model in engineering, such as the way to obtain continuous decomposition fields for the closure terms in complicated flows, and the advanced technology to detect multi-valued phenomenon in a complex high-dimensional training data. Also in the midst of actual operations, special input features such as λ used in the input feature space would cause a numerical instability during the iterative process, indicating the dynamic properties of the differential system near the fixed point designed in this study needs to be further studied.

Appendix A. The Entire Tensor Bases for Algebraic Stress Model

The full expression in the explicit constitutive equation can be found as follows:

$$\mathbf{b}^* = \sum_{m=1}^{10} G^{(m)}(\lambda_1, \dots, \lambda_5) \mathbf{T}^{(m)} \quad (\text{A.1})$$

where the definition of $\mathbf{T}^{(m)}$ and λ is defined as:

$$T^{(m)} = \begin{cases} T^{(1)} = S^* & T^{(6)} = \Omega^* S^{*2} + S^{*2} \Omega^* - 2/3 E \cdot tr(S^* \Omega^{*2}) \\ T^{(2)} = S^* \Omega^* - \Omega^* S^* & T^{(7)} = \Omega^* S^* \Omega^{*2} - \Omega^{*2} S^* \Omega^* \\ T^{(3)} = S^{*2} - 1/3 E \cdot tr(S^{*2}) & T^{(8)} = S^* \Omega^* S^{*2} - S^{*2} \Omega^* S^* \\ T^{(4)} = \Omega^{*2} - 1/3 E \cdot tr(\Omega^{*2}) & T^{(9)} = \Omega^{*2} S^{*2} + S^{*2} \Omega^{*2} - 2/3 E \cdot tr(S^{*2} \Omega^{*2}) \\ T^{(5)} = \Omega^* S^{*2} - S^{*2} \Omega^* & T^{(10)} = \Omega^* S^{*2} \Omega^{*2} - \Omega^{*2} S^{*2} \Omega^* \end{cases},$$

$$\lambda_1 = tr(S^{*2}), \lambda_2 = tr(\Omega^{*2}), \lambda_3 = tr(S^{*3}), \lambda_4 = tr(\Omega^{*2} S^*), \lambda_5 = tr(\Omega^{*2} S^{*2}).$$

Acknowledgements

The authors would like to dedicate this paper to Prof. Lipeng Lu, the supervisor of Weishuo Liu and Jian Fang, who has left us in February 2019. He devoted all his life studying the mystery in turbulence flow and was always caring for everything about his students beyond academic affairs. This work would not have been done without his contribution and academic outlook. We will long remember his elegance, kindness, demeanor, and optimism fighting against fatal illness. The project is supported by the National Natural Science Foundation of China (Grant Nos. 51420105008). The authors would also like to acknowledge UKRI-EPSRC under Grant Nos. EP/L000261/1 and EP/K024574/1 for their financial support.

References

References

- [1] J. Slotnick, A. Khodadoust, J. Alonso, D. Darmofal, W. Gropp, E. Lurie, D. Mavriplis, Cfd vision 2030 study: a path to revolutionary computational aerosciences, Tech. rep. (2014).
- [2] M. M. Rogers, Progress towards the cfd vision 2030, Tech. rep. (2018).
- [3] B. E. Launder, G. J. Reece, W. Rodi, Progress in the development of a reynolds-stress turbulence closure, Journal of fluid mechanics 68 (3) (1975) 537–566.
- [4] B. E. Launder, B. Sharma, Application of the energy-dissipation model of turbulence to the calculation of flow near a spinning disc, Letters in heat and mass transfer 1 (2) (1974) 131–137.
- [5] F. R. Menter, Two-equation eddy-viscosity turbulence models for engineering applications, AIAA Journal 32 (8) (1994) 1598–1605. doi:10.2514/3.12149.
- [6] F. R. Menter, M. Kuntz, R. Langtry, Ten years of industrial experience with the sst turbulence model, Turbulence, heat and mass transfer 4 (1) (2003) 625–632.
- [7] P. Spalart, S. Allmaras, A one-equation turbulence model for aerodynamic flows, in: 30th aerospace sciences meeting and exhibit, p. 439.
- [8] S. Wallin, A. Johansson, An explicit algebraic reynolds stress model for incompressible and compressible turbulent flows, Journal of Fluid Mechanics 403 (2000) 89–132.
- [9] D. C. Wilcox, Formulation of the k-w turbulence model revisited, AIAA Journal 46 (11) (2008) 2823–2838. doi:10.2514/1.36541.

- [10] D. C. Wilcox, Turbulence modeling for CFD, Vol. 2, DCW industries La Canada, CA, 1998.
- [11] S. Kline, B. Cantwell, G. Lilley, Complex turbulent shear flows: comparison of computation and experiment, Thermosciences Division, Mech. Engg. Dept., Stanford (1982).
- [12] Y. Liu, X. Yu, B. Liu, Turbulence models assessment for large-scale tip vortices in an axial compressor rotor, *Journal of Propulsion and Power* 24 (1) (2008) 15–25.
- [13] F. Villalpando, M. Reggio, A. Ilinca, Assessment of turbulence models for flow simulation around a wind turbine airfoil, *Modelling and simulation in Engineering* 2011 (2011) 6.
- [14] C. J. Roy, F. G. Blottner, Review and assessment of turbulence models for hypersonic flows, *Progress in Aerospace Sciences* 42 (7-8) (2006) 469–530.
- [15] D. Michie, D. J. Spiegelhalter, C. Taylor, *Machine learning, Neural and Statistical Classification* 13 (1994).
- [16] K. Duraisamy, G. Iaccarino, H. Xiao, Turbulence modeling in the age of data, *Annual Review of Fluid Mechanics* 51 (1) (2019) 357–377. doi:10.1146/annurev-fluid-010518-040547.
- [17] J. N. Kutz, Deep learning in fluid dynamics, *Journal of Fluid Mechanics* 814 (2017) 14. doi:10.1017/jfm.2016.803.
- [18] P. A. Durbin, Some recent developments in turbulence closure modeling, *Annual Review of Fluid Mechanics* 50 (1) (2018) 77–103. doi:10.1146/annurev-fluid-122316-045020.
- [19] E. J. Parish, K. Duraisamy, A paradigm for data-driven predictive modeling using field inversion and machine learning, *Journal of Computational Physics* 305 (2016) 758–774. doi:10.1016/j.jcp.2015.11.012.
- [20] J. R. Holland, J. D. Baeder, K. Duraisamy, Towards integrated field inversion and machine learning with embedded neural networks for rans modeling, in: *AIAA Scitech 2019 Forum*, 2019, p. 1884.
- [21] A. P. Singh, S. Medida, K. Duraisamy, Machine-learning-augmented predictive modeling of turbulent separated flows over airfoils, *AIAA Journal* (2017) 2215–2227.
- [22] K. Duraisamy, Z. J. Zhang, A. P. Singh, New Approaches in Turbulence and Transition Modeling Using Data-driven Techniques. arXiv:<https://arc.aiaa.org/doi/pdf/10.2514/6.2015-1284>, doi:10.2514/6.2015-1284.
URL <https://arc.aiaa.org/doi/abs/10.2514/6.2015-1284>
- [23] B. D. Tracey, K. Duraisamy, J. J. Alonso, A Machine Learning Strategy to Assist Turbulence Model Development. arXiv:<https://arc.aiaa.org/doi/pdf/10.2514/6.2015-1287>, doi:10.2514/6.2015-1287.
URL <https://arc.aiaa.org/doi/abs/10.2514/6.2015-1287>
- [24] K. Duraisamy, P. Durbin, Transition modeling using data driven approaches, in: *CTR Summer Program*, 2014, p. 427.
- [25] L. Zhu, W. Zhang, J. Kou, Y. Liu, Machine learning methods for turbulence modeling in subsonic flows around airfoils, *Physics of Fluids* 31 (1) (2019) 015105.
- [26] S. B. Pope, A more general effective-viscosity hypothesis, *Journal of Fluid Mechanics* 72 (2) (1975) 331–340. doi:10.1017/S0022112075003382.
- [27] J. Lumley, Toward a turbulent constitutive relation, *Journal of Fluid Mechanics* 41 (2) (1970) 413–434.
- [28] A. J. M. Spencer, R. S. Rivlin, The theory of matrix polynomials and its application to the mechanics of isotropic continua, *Archive for rational mechanics analysis* 2 (1) (1958) 309–336.
- [29] A. J. Spencer, R. S. Rivlin, Further results in the theory of matrix polynomials, *Archive for rational mechanics analysis* 4 (1) (1959) 214–230.
- [30] J. Weatheritt, R. Sandberg, A novel evolutionary algorithm applied to algebraic modifications of the rans stress-strain relationship, *Journal of Computational Physics* 325 (2016) 22–37. doi:10.1016/j.jcp.2016.08.015.
- [31] J. Weatheritt, R. Sandberg, The development of algebraic stress models using a novel evolutionary algorithm, *International Journal of Heat and Fluid Flow* 68 (2017) 298–318.
- [32] H. Akolekar, J. Weatheritt, N. Hutchins, R. Sandberg, G. Laskowski, V. Michelassi, Development and use of machine-learned algebraic reynolds stress models for enhanced prediction of wake mixing in low-pressure turbines, *Journal of Turbomachinery* 141 (4) (2019) 041010.

- [33] J. Ling, A. Kurzawski, J. Templeton, Reynolds averaged turbulence modelling using deep neural networks with embedded invariance, *Journal of Fluid Mechanics* 807 (2016) 155–166. doi:10.1017/jfm.2016.615.
- [34] J. Ling, R. Jones, J. Templeton, Machine learning strategies for systems with invariance properties, *Journal of Computational Physics* 318 (2016) 22–35. doi:10.1016/j.jcp.2016.05.003.
- [35] J.-X. Wang, J.-L. Wu, H. Xiao, Physics-informed machine learning approach for reconstructing reynolds stress modeling discrepancies based on dns data, *Physical Review Fluids* 2 (3) (2017) 034603. doi:10.1103/PhysRevFluids.2.034603.
URL <https://link.aps.org/doi/10.1103/PhysRevFluids.2.034603>
- [36] J.-L. Wu, H. Xiao, E. Paterson, Physics-informed machine learning approach for augmenting turbulence models: A comprehensive framework, *Physical Review Fluids* 3 (7) (2018) 074602. doi:10.1103/PhysRevFluids.3.074602.
URL <https://link.aps.org/doi/10.1103/PhysRevFluids.3.074602>
- [37] J. Wu, H. Xiao, R. Sun, Q. Wang, Reynolds-averaged navierstokes equations with explicit data-driven reynolds stress closure can be ill-conditioned, *Journal of Fluid Mechanics* 869 (2019) 553–586. doi:10.1017/jfm.2019.205.
- [38] S. V. Patankar, *Numerical heat transfer and fluid flow*, hemisphere publ, Corp., New York 58 (1980).
- [39] J. H. Ferziger, M. Perić, R. L. Street, *Computational methods for fluid dynamics*, Vol. 3, Springer, 2002.
- [40] R. L. Thompson, L. E. B. Sampaio, F. A. de Bragana Alves, L. Thais, G. Mompean, A methodology to evaluate statistical errors in dns data of plane channel flows, *Computers & Fluids* 130 (2016) 1 – 7. doi:<https://doi.org/10.1016/j.compfluid.2016.01.014>.
URL <http://www.sciencedirect.com/science/article/pii/S0045793016300068>
- [41] T. Craft, B. Launder, K. Suga, Development and application of a cubic eddy-viscosity model of turbulence, *International Journal of Heat and Fluid Flow* 17 (2) (1996) 108–115.
- [42] H. Abe, H. Kawamura, Y. Matsuo, Direct numerical simulation of a fully developed turbulent channel flow with respect to the reynolds number dependence, *Journal of Fluids Engineering* 123 (2) (2001) 382–393. doi:10.1115/1.1366680.
URL <https://doi.org/10.1115/1.1366680>
- [43] M. H. Hassoun, et al., *Fundamentals of artificial neural networks*, MIT press, 1995.
- [44] M. Shinki, K. Shimizu, Approximation of inverse system (many-valued function) by neural network, *Electronics and Communications in Japan (Part III: Fundamental Electronic Science)* 84 (8) (2001) 57–66.
- [45] R. Fang, D. Sondak, P. Protopapas, S. Succi, Neural network models for the anisotropic reynolds stress tensor in turbulent channel flow, *Journal of Turbulence* (2019) 1–19.
- [46] H. G. Weller, G. Tabor, H. Jasak, C. Fureby, A tensorial approach to computational continuum mechanics using object-oriented techniques, *Computers in Physics* 12 (6) (1998). doi:10.1063/1.168744.
- [47] S. V. Patankar, D. B. Spalding, A calculation procedure for heat, mass and momentum transfer in three-dimensional parabolic flows, in: *Numerical prediction of flow, heat transfer, turbulence and combustion*, Elsevier, 1983, pp. 54–73.
- [48] M. Abadi, P. Barham, J. Chen, Z. Chen, A. Davis, J. Dean, M. Devin, S. Ghemawat, G. Irving, M. Isard, Tensorflow: A system for large-scale machine learning, in: *12th Symposium on Operating Systems Design and Implementation*, pp. 265–283.
- [49] T. Chen, M. Li, Y. Li, M. Lin, N. Wang, M. Wang, T. Xiao, B. Xu, C. Zhang, Z. Zhang, Mxnet: A flexible and efficient machine learning library for heterogeneous distributed systems, *arXiv: Distributed, Parallel, Cluster Computing* (2015).
- [50] Y. Jia, E. Shelhamer, J. Donahue, S. Karayev, J. Long, R. Girshick, S. Guadarrama, T. Darrell, Caffe: Convolutional architecture for fast feature embedding, *arXiv preprint arXiv:1408.5093* (2014).
- [51] F. Pedregosa, G. Varoquaux, A. Gramfort, V. Michel, B. Thirion, O. Grisel, M. Blondel, P. Prettenhofer, R. Weiss, V. Dubourg, et al., Scikit-learn: Machine learning in python, *Journal of machine learning research* 12 (Oct) (2011) 2825–2830.

- [52] L. Weishuo, F. Jian, An interface of tensorflow and openfoam for ai supported physical simulations, in preparation.
- [53] R. D. Moser, J. Kim, N. N. Mansour, Direct numerical simulation of turbulent channel flow up to $Re_\tau = 590$, *Physics of fluids* 11 (4) (1999) 943–945.
- [54] P. Balakumar, G. I. Park, Dns/les simulations of separated flows at high reynolds numbers, in: 45th AIAA Fluid Dynamics Conference, 2015, p. 2783.
- [55] R. Tibshiranit, Regression shrinkage and selection via the lasso, *Journal of the royal statistical society series b-methodological* 58 (1) (1996) 267–288.
- [56] R. B. Dean, Reynolds number dependence of skin friction and other bulk flow variables in two-dimensional rectangular duct flow, *Journal of Fluids Engineering-transactions of The Asme* 100 (2) (1978) 215–223.